Heterogeneous Structure in Gas–Solid Riser Flows

Jun You and Chao Zhu
Dept. of Mechanical Engineering, New Jersey Institute of Technology, Newark, NJ 07102

Bing Du and Liang-Shih Fan
Dept. of Chemical and Biochemical Engineering, Ohio State University, Columbus, OH 43210

DOI 10.1002/aic.11488
Published online April 22, 2008 in Wiley InterScience (www.interscience.wiley.com).

Recent measurements by electric capacitance tomography reveal that, under certain operating conditions, the solids concentration distribution in the dense and acceleration regimes of gas–solid riser flows exhibits a strong heterogeneous structure, with the solids concentration near the centerline much higher than that in the annular surrounding flows (except in the wall region) within the same cross-section. This core–annulus–wall heterogeneous structure, significantly different from the commonly known "core–annulus (wall)" two-zone structure in riser flows, becomes unstable with the increase in solids loading, which eventually leads to the occurrence of choking. In this study, we propose a mechanistic model to investigate the formation and distribution of these interesting heterogeneous structures in riser flows. The intrinsic mechanisms include (1) counterflow between back mixing solids and upward moving solids from entrance, (2) the radial migration of solid flow from the wall toward the centerline of riser, and (3) the nonuniform acceleration of solids across the cross-section in the dense and acceleration regimes. The model, assuming one-dimensional two-phase flow in each zone along the riser, consists of a set of coupled ordinary-differential equations developed from the conservation laws of mass, momentum, and energy of both gas and solids phases. The solving algorithm is based on the Runge-Kutta method. Our model calculations show that the commonly known "core–annulus (wall)" flow structure occurs at low solids loadings and/or high gas velocities, whereas the core–annulus–wall flow structure is formed at moderate solids loading and/or at low gas velocities. With a high solids loading at low gas velocity, severe backflow results in a solid concentration peak formed in the core, which not only causes the flow instability but also possibly triggers the choking. Model simulations are validated by direct comparisons against measurements in solids concentrations as well as in the pressure drop along the riser, which shows a fairly good agreement. © 2008 American Institute of Chemical Engineers *AIChE J*, 54: 1459–1469, 2008

Keywords: heterogeneous structure, gas–solid riser flow, dense phase, acceleration

Introduction

Gas–solids riser flows can be found in many industrial applications, including fluidized catalytic cracking, circulating fluidized bed combustion, polymerization, chemical syn-

Correspondence concerning this article should be addressed to C. Zhu at zhu@adm.njit.edu.

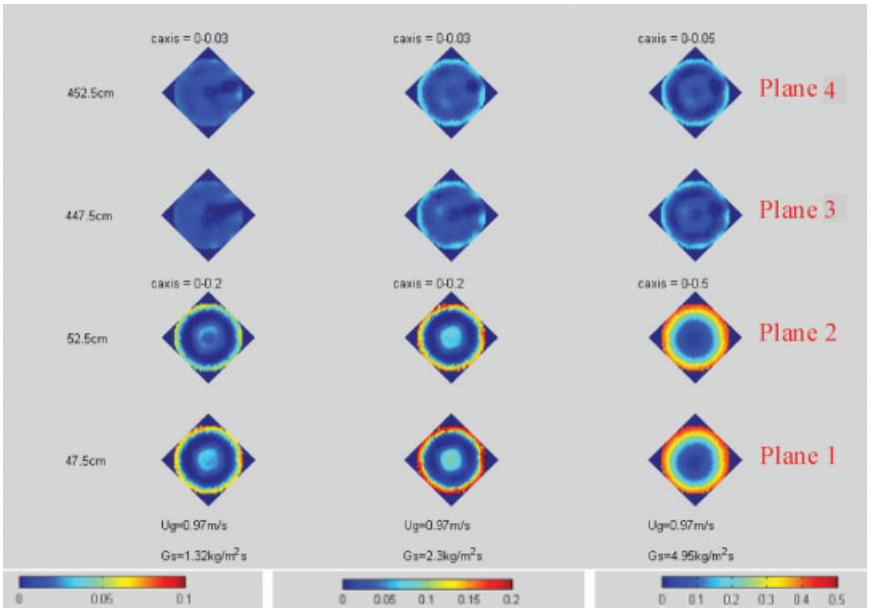

Figure 1. Wall–annulus–core structure in CFB.[10]

[Color figure can be viewed in the online issue, which is available at www.interscience.wiley.com.]

thesis, and vertical pneumatic transport of solids.[1] In a gas–solids riser flow, the hydrodynamic flow characteristics of both gas and solids phases can be strongly heterogeneous, represented by the nonuniform distributions of solids concentration and phase velocities in both the axial and radial directions. The axial nonuniformity is due to the phase acceleration, whereas the radial uniformity is mainly caused by the wall boundary effect.

The heterogeneous flow structure has been poorly understood, mainly because of the lack of appropriate measurement techniques applicable to gas–solid riser flows at moderate or high solids loadings, especially in the riser bottom where the dense and acceleration regimes are located. The cross-section averaged distribution of solids holdup along the riser is commonly estimated from the pressure drop measurements by assuming the solids in a fully developed suspension state without acceleration, which is probably true for gas–solid flows in the dilute transport regime in the upper part of riser yet away from the riser exit. The local solids holdup can be estimated either from the intrusive probe measurements (e.g., optical fiber probe[2]; capacitance probe[3,4]) or from the nonintrusive measurements (e.g., X-ray imaging[5]; γ-ray imaging[6]; laser-sheet imaging[7]; tomography[8,9]). Most of these techniques fail to yield accurate and instantaneous measurements for a precise description of the flow structure in a gas–solids riser flow, especially near the wall region or in the riser bottom. The recently developed electrical capacitance tomography (ECT) appears to be the most promising tomography technique for the flow structure diagnosis of gas–solid riser flows, with a much improved spatial and temporal imaging resolution.[9] Despite the lack of accurate measurements, it has become a common understanding that the heterogeneous flow structure in a cross section of riser can be, in general, described by a core–annular structure, in which the upwards moving solids are in the core, whereas a dense layer of solids, mostly likely downwards moving, is in the wall (or annular) region. The solids concentration decreases monotonically toward the center of the cross-section, whereas the solids velocity increases monotonically toward the center. The solid concentration monotonically decreases along the riser, typically in an S-shape, where the transition from dense phase to dilute phase is due to the solids acceleration. This core–annular cross-section structure with an S-shaped axial distribution, however, does not give a clear explanation of the flow structure in the bottom of riser, where the downwards moving solids from the wall is conceptually mixed with the upwards moving solids from the riser entrance. Neither can the core–annular structure model explain the choking–a critical transition of flow structure (and solids transport) that occurs typically in relatively small-sized risers at low transport velocities with moderate solids loadings.

Our recent measurements using ECT reveal that, under certain operating conditions, a radial symmetry of the time-averaged solids holdup distribution, and shows that there exists a double ring structure in solids concentration in a circulating fluidized bed riser.[10] As shown in Figure 1, in the dense and acceleration regimes (represented by Planes 1 or 2), the solids concentration is much denser than that in the annulus (except in the wall region). This core–annulus–wall heterogeneous structure, significantly different from the commonly known "core–annulus (wall)" two-zone structure in riser flows, becomes unstable with the increase in solids loading, which eventually leads to the occurrence of choking[10]. In the dilute transport regime (represented by Planes 3 or 4), the solids concentrations, however, follow very much the "core–annulus (wall)" two-zone structure. Such findings are very interesting, because they indicate that the radial profile for some dense phase riser flows could be of a core–annulus–wall three-region structure rather than the widely accepted core–annulus (wall) two-region structure.

Most models of heterogeneous flow structure are based on the core–annulus (wall) flows,[11–15] which typically consider a dilute uniform core flow, and a dense wall flow along the riser.

These models fail to provide the detailed mechanisms in the bottom region of riser where the flows can be very dense and complex. A primitive model was lately proposed to interpret the reported core–annulus–wall structure,[16] using a simplified kinetic theory model to account for the solids acceleration in collision dominated dense flow regimes near the bottom of riser. It is apparent, however, that the most traditional momentum-based models with the assistance of a kinetic theory modeling approach may be insufficient to describe some basic physics of collision-induced energy dissipation in fluidization, such as energy dissipations from tangential slip and rotational slip. This deficiency may be represented by the inability to correctly predict the pressure distribution in the dense flow regime near the bottom of a circulating fluidized bed (CFB) riser. The importance of correct account of energy transport and dissipation in the momentum equation may be analogous to that of k-ε model in the turbulent momentum transport equations in turbulence flows. Hence, an additional term due to energy dissipation should be introduced into the solid momentum transport equation in the collision and acceleration dominated regime.[17]

This paper aims to present a complete study on the formation mechanisms of the heterogeneous structure (especially the core–annulus–wall structure) in gas–solids risers using both experimental and theoretical approaches. First we will propose the physical mechanisms for the formation of various heterogeneous structures in riser flows, including the mechanisms leading to choking. Then we will outline a mechanistic three-zone model, which is developed based on various conservation equations as well as constitutive correlations from the proposed mechanisms. By further assuming a one-way coupling of phase interactions between the wall and core–annulus regions, a simplified model simulation is performed over a wide range of operating conditions. The modeling predictions are then verified against ECT measurements, in which the solids concentration distributions and pressure drop distributions are directly compared. Parametrical effects of solids loadings and gas transport velocities are discussed to illustrate the characteristic differences of heterogeneous flow structures among the core–annular (wall) two-zone structure, the core–annulus–wall three-zone structure, and the unstable structures leading to choking.

Formation Mechanisms of Hetereous Flow Structure

Let us examine the phenomenological structures of gas–solids riser flows with uniform inlet flow conditions, as shown in Figure 2. The commonly understood parts of the heterogeneous flow structure consist a dilute phase transport in the core–annulus region near the top of the riser, a dense phase transport in the core–annulus region near the bottom of the riser, a layer of downwards moving solids near the wall for most part of the riser except for the entrance region, and a uniform upwards moving gas–solids flow at the riser inlet. The parts of the heterogeneous flow structure that require further explanation include the detailed flow structural and behavioral information right after the flow entrance, the counterflow mixing between the downwards moving solids and the upwards moving solids in the wall region near the entrance, the structural transition in the solids acceleration region, and the flow structure dependency of the pressure drop distribution.

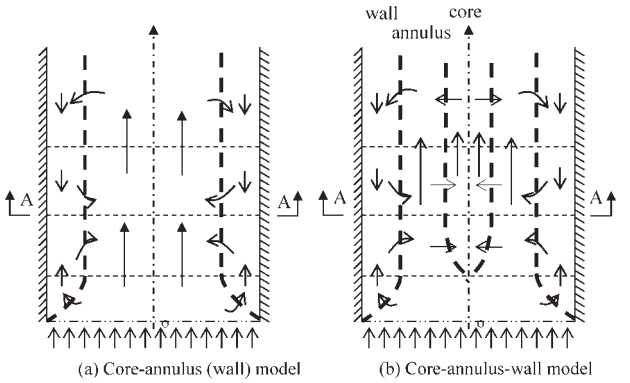

Figure 2. Heterogeneous flow structures in risers.

(a) Core–annulus (wall) model; (b) core–annulus–wall model.

From the phenomenological consideration, a wall region of dense solids concentration has to be developed from the riser bottom, because the averaged gas velocity in the wall region becomes too low to support upward moving solids due to the friction between riser wall and gas–solids flow. At a certain bed height, the solids in the wall region have to exhaust all their initial upward momentum and begin to fall due to gravity. At this location, the averaged solids velocity in the wall region is null. Thus, in the bed section near this height, all solids from the upper wall region or from the lower wall region are forced to migrate inwardly towards the riser column center.[15] In a high convection riser flow (i.e., at a high fluidization velocity and low solids loading) with little or moderate backflow of solids, the inwardly migrating solids are all entrained into the flow with few residual solids reaching the center of the riser. In this case, the flow pattern is commonly known as "core–annulus" two-region flow, where the radial solids concentration gradually decreases toward the centerline of riser, as illustrated in Figure 2a.

In other cases, especially with low fluidization velocities, part of the inwardly migrating solids may reach the central axis of riser. Because of the axial symmetry of a cylindrical riser, a dense core region must be formed, as shown in Figure 2b. Required by a nearly equal axial pressure gradient in all regions at the same bed height, the gas velocity in the core tends to be lower than that in the annulus where the solids concentration is relatively leaner. The slower moving gas in the core results in a lower acceleration of solids in the core region, and hence preserves this core–annulus–wall structure with a relatively higher solids concentration at the core along the riser. In the mean time, based on the mass balance of solids, the downwards moving solids in the wall region in the upper part of a riser must come from those solids in the annulus and core. Hence, in the upper part of the riser, the solids migration into the wall yields depletion in solids concentration, which is severer in the core than in the annulus. Therefore, near the top of a riser, a core–annulus–wall structure technically still exists, yet it resembles the commonly known core–annulus two-zone structure. Thus, the formation mechanisms of the core–annulus and core–annulus–wall structures can be fully explained.

Figure 3 shows the schematic radial distributions of solids concentrations and solids velocities at an imaginary *A–A*

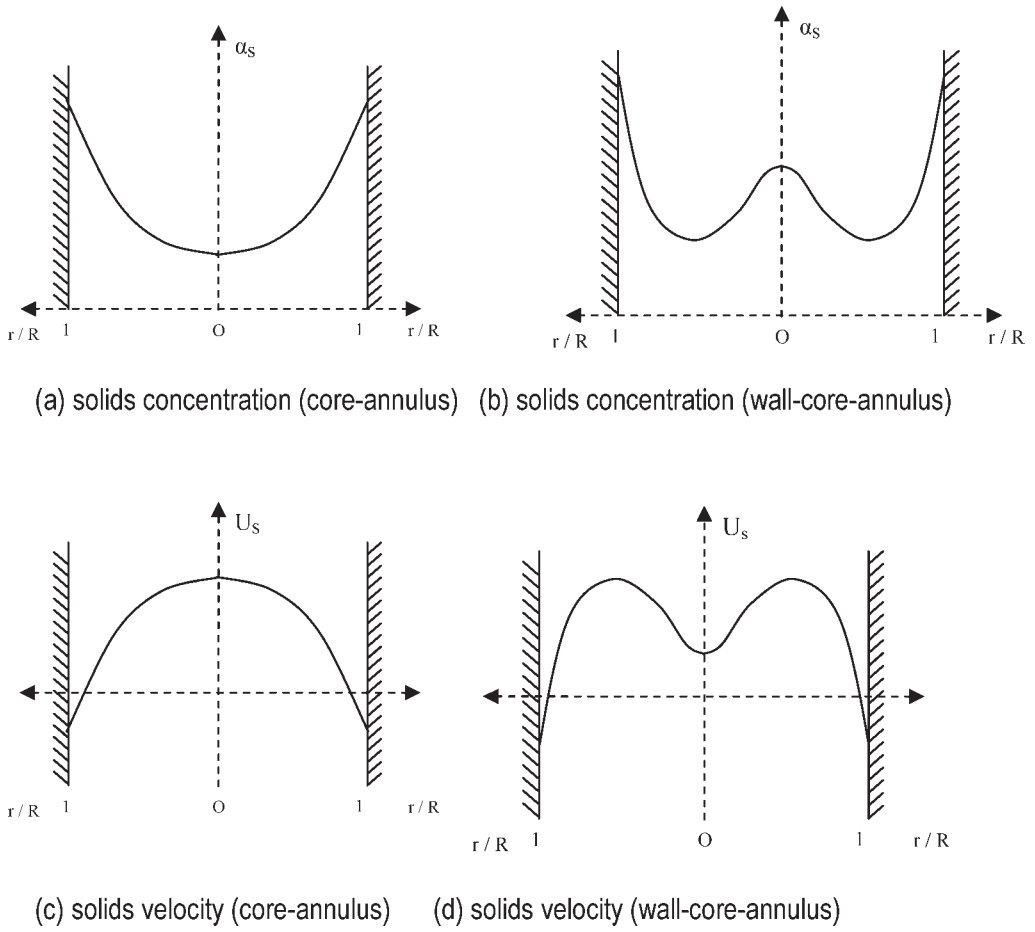

Figure 3. Radial distributions of solids phase (in *A* - *A* plane).

(a) Solids concentration (core–annulus). (b) Solids concentration (wall–core–annulus). (c) Solids velocity (core–annulus). (d) Solids velocity (wall–core–annulus).

plane in Figure 2. The core–annulus structure has a typical paraboloidal distribution of solids concentration at any cross section, with the solid concentration in the wall region much higher than that in the core, as shown in Figure 3a. Whereas, for the new revealed wall–core–annulus structure, there is a peak in solid concentration in the core region. Even with the peak in the core, the solids concentration in the wall may still be the highest in the cross section, as shown in Figure 3b. Accordingly, the radial distributions solids velocities are illustrated in Figures 3c, d, respectively, for cases of core–annular structure and core–annulus–wall structure. It is noted that, because of the wall friction and effect of boundary layers, the solid velocity close to the wall in both structures is not only much lower than that in central of the riser, but also downwards moving under gravity. In a flow with the core–annulus structure, the highest solid velocity is located in the center of the riser flow, whereas for a flow with the wall–core–annulus structure, solid velocities in both wall and core region are lower than that in the annulus region.

Three-Zone Modeling

In reality the solids concentration distributions in both radial and axial directions should be continuous, which indicates that a set of partial differential equations of variants with respect to both radial and axial coordinates must be dealt with in a complete hydrodynamic modeling of gas–solid riser flows. A typical radial profile of solids concentration based on the optical probe measurements is shown in Figure 4, which demonstrates that, although the actual radial distribution is continuous, the profile can also be approximated, for the sake of simplicity, by a simple piecewise-uniform distribution in a three-zone structure. On the basis of

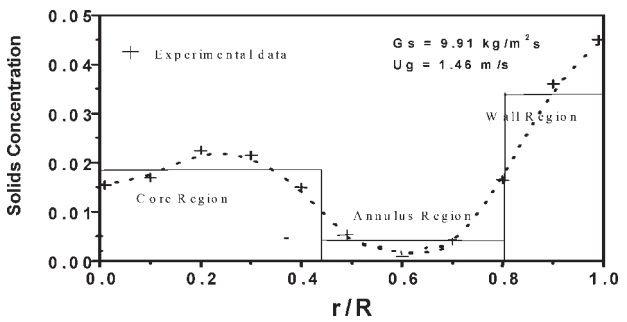

Figure 4. Three-zone representation of solids concentration distribution.[10]

this approximation as well as observations from ECT measurements, we further assume that the basic form of piecewise-uniform radial distribution is not only applicable to the entire riser but also applicable to all gas–solid flow properties, so that the hydrodynamic model can be approximated by a set of ordinary differential equations that depend only upon the axial coordinate of riser.

Based on the core–annulus–wall flow structure with piecewise-uniform radial distributions, independent governing equations can now be established for gas velocities, solid velocities, and solid volume fractions in the entire region of riser. A summary of these equations are given as follows. Notations are referred to the section of list of symbols.

Geometric relations and equation of state

$$A = A_c + A_a + A_w \tag{1}$$

$$\rho = \frac{P}{RT} \tag{2}$$

$$\alpha_i + \alpha_{si} = 1, \quad i = a, c, w \tag{3}$$

Mass balance of solids

Overall balance:

$$G_s A = \rho_s \alpha_{sc} U_{sc} A_c + \rho_s \alpha_{sa} U_{sa} A_a + \rho_s \alpha_{sw} U_{sw} A_w \tag{4}$$

Core region:

$$\frac{d}{dz}(\alpha_{sc} \rho_s U_{sc} A_c) = \dot{m}_{sc} \tag{5}$$

Annulus region:

$$\frac{d}{dz}(\alpha_{sa} \rho_s U_{sa} A_a) = \dot{m}_{sw} - \dot{m}_{sc} \tag{6}$$

Wall region:

$$\frac{d}{dz}(\alpha_{sw} \rho_s U_{sw} A_w) = -\dot{m}_{sw} \tag{7}$$

Mass balance of gas

$$GA = \rho \alpha_c U_c A_c + \rho \alpha_a U_a A_a + \rho \alpha_w U_w A_w \tag{8}$$

Gas momentum balance

Overall:

$$\frac{d}{dz}\left(\sum_{i=a,c,w} \alpha_i \rho U_i^2 A_i\right) = -\frac{dp}{dz} A - \sum_{i=a,c,w} F_{Di} A_i - \sum_{i=a,c,w} \alpha_i \rho g A_i - F_{fww} \tag{9}$$

Core region:

$$\frac{d}{dz}(\alpha_c \rho U_c^2 A_c) = -\frac{dp}{dz} A_c - F_{DC} A_c - \alpha_c \rho g A_c - F_{fac} \tag{10}$$

Annulus region:

$$\frac{d}{dz}(\alpha_A \rho U_A^2 A_A) = -\frac{dp}{dz} A_A - F_{DA} A_A - \alpha_A \rho g A_A + F_{fac} - F_{faw} \tag{11}$$

Wall region:

$$\frac{d}{dz}(\alpha_w \rho U_w^2 A_w) = -\frac{dp}{dz} A_w - F_{DW} A_W - \alpha_w \rho g A_w - F_{fww} + F_{faw} \tag{12}$$

Momentum balance of solids

$$\frac{d}{dz}\left(\sum_{i=a,c,w} \alpha_{si} \rho_s U_{si}^2 A_i\right) = \sum_{i=a,c,w} F_{Di} A - \sum_{i=a,c,w} \alpha_{si} \rho_s g A_i + \sum_{i=a,c,w} \frac{d}{dz}\left(C_{ppi} \frac{dU_{si}}{dz}\right) - F_{fsw} \tag{13}$$

Core region:

$$\frac{d}{dz}(\alpha_{sc} \rho_s U_{sc}^2 A_c) = F_{DC} A_c - \alpha_{sc} A_c \rho_s g + \frac{d}{dz}\left(C_{ppc} \frac{dU_{sc}}{dz}\right) + \dot{m}_{sc} U_{sc} \tag{14}$$

Annulus region:

$$\frac{d}{dz}(\alpha_{sa} \rho_s U_{sa}^2 A_a) = F_{DA} A_a - \alpha_{sa} A_a \rho_s g + \frac{d}{dz}\left(C_{ppa} \frac{dU_{sa}}{dz}\right) - \dot{m}_{sc} U_{sa} + \dot{m}_{sw} U_{sw} \tag{15}$$

Wall region:

$$\frac{d}{dz}(\alpha_{sw} \rho_s U_{sw}^2 A_w) = F_{DW} A_w - \alpha_{sw} A_w \rho_s g + \frac{d}{dz}\left(C_{ppw} \frac{dU_{sw}}{dz}\right) - \dot{m}_{sw} U_{sw} - F_{fsw} \tag{16}$$

Definition of regional boundaries

Based on the ECT measurements,[10] the zone areas appear to have little variation along the riser, so that we may assume that

$$\frac{dA_w}{dz} = 0 \tag{17}$$

$$\frac{A_c}{A_a} = \text{constant} \tag{18}$$

In summary, for a complete description of the core–annulus–wall model of gas–solid riser flows, we have 14 independent equations [(1)–(3), (5)–(8), (10)–(12), (14)–(16) and (18)] for 14 independent variables (A_c, A_w, A_a, U_{sc}, U_{sa}, U_{sw}, α_{sc}, α_{sa}, α_{sw}, U_c, U_a, U_w, p, ρ). Hence, the problem is closed. However, in order to solve for a specific gas–solid riser flow application, the detailed flow boundary conditions and flow operation conditions, as well as intrinsic correlations for interzone transport (e.g., F_f's), multiphase interactions (e.g., F_D's) and transport coefficients within the same phase (e.g., C_p's), must be specified.

Simplified Three-Zone Model

To further simplify the problem, we adopt the one-way flow coupling between the wall region and the core–annulus region. Namely, the gas–solid flows in the wall region are predetermined from wall boundary conditions and decoupled from the governing equations of the core and annulus region. Why do we need to adopt this approach? First, there is no mature hydrodynamic model to describe the complicated mechanisms of gas–solid-wall friction and multiphase interactions in the wall boundary layer region, where a dense layer of moving solids is present. Second, the distribution of solids backflow in the all region along the riser is difficult to determine due to the lack of sufficient measurements and little understanding about turbulent transport of solids across the wall boundary layer. Third, little has been modeled on the hydrodynamics of gas flow in the wall boundary layer with a dense solids suspension. With such a one-way coupling simplification, the coupled set of ordinary differential equations becomes associated only with a core–annulus gas–solid flow and with a given axial distribution of solids migration from the wall region along the riser. Hence, the complexity of the problem is greatly reduced.

Flow characteristics in the wall region

Schematic distributions of the solids flow in the wall region along a riser are depicted in Figure 5, with (a) for the cross-section area of wall zone, (b) for the solids volume fraction, (c) for the solids mass flux across the wall–annulus boundary, (d) for the solids velocity, and (e) for the wall–entrance region. The characteristic heights of Z_e, Z_1, Z_2, and Z_3 denote, respectively, the end location of entrance regime, the end location of upwards moving solids in the wall region, the end location of radial-inwards migrating solids in the wall region, and the height of riser.

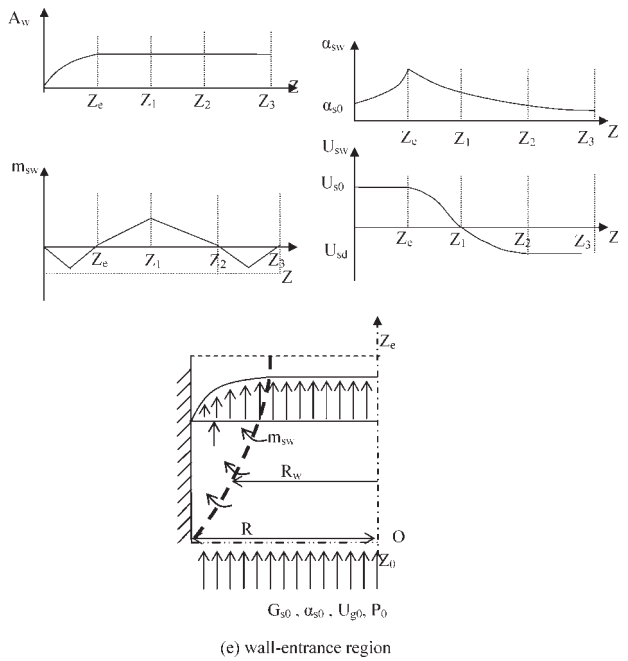

Figure 5. Schematic profiles of solids flow in the wall region.

Based on the mass continuity and flow characteristics, the distributions of solids mass flux across the wall–annulus boundary must satisfy the following conditions:

$$\int_{z_1}^{z_2} \dot{m}_{sw}\, dz = \int_{z_2}^{z_3} \dot{m}_{sw}\, dz \tag{19}$$

$$\int_{z_0}^{z_1} \dot{m}_{sw}(z)\, dz = \int_{z_e}^{z_1} \dot{m}_{sw}(z)\, dz = G_{swe} \cdot A_w \tag{20}$$

$$\int_{z_1}^{z_2} \dot{m}_{sw}\, dz = \int_{z_2}^{z_\infty} \dot{m}_{sw}\, dz = G_{sB} A_w \tag{21}$$

The distribution of solids velocity must satisfy the following conditions:

$$U_{sw}|_{z=Z_1} = 0 \quad \text{and} \quad \left.\frac{dU_{sw}}{dz}\right|_{z=Z_1} < 0 \tag{22}$$

$$\dot{m}_{sw}|_{z=0} = \dot{m}_{sw}|_{z=Z_\emptyset} = \dot{m}_{sw}|_{z=Z_2} = 0 \tag{23}$$

$$\left.\frac{d\dot{m}_{sw}}{dz}\right|_{z=Z_e} > 0 \quad \text{and} \quad \left.\frac{d\dot{m}_{sw}}{dz}\right|_{z=Z_2} < 0 \tag{24}$$

It is noted that the distributions of cross-section area of wall zone, solids concentration, solids velocity, and solids mass flux across the wall–annulus boundary are not independent of each other. Once three of them are determined, the remaining one can be deduced from the mass conservation of solids. In this study, we choose to predefine the distributions of cross-section area of wall zone, solids velocity, and solids mass flux across the wall–annulus boundary, whereas the distribution of the solid concentration is derived from the other three. This kind of selection has the advantage that the derived solids concentration distribution with the available experimental data (such as from ECT measurements) can be checked and validated or determined through common sense at the bulk range.

The distributions of solids velocity and solids mass flux across the wall–annulus boundary are assumed as follows, which satisfy the integral or boundary conditions of Eqs. 19–24.

$$U_{sw} = \begin{cases} U_{s0}\left[-1+e^{-U_{sd}\left(\frac{Z_1}{z}-1\right)}\right] & 0 \le z \le Z_1 \\ U_{sd}\left[-1+e^{-U_{s0}\left(\frac{z}{Z_1}-1\right)}\right] & Z_1 \le z \le Z_3 \end{cases} \tag{25}$$

$$\dot{m}_{sw}(z) \begin{cases} \frac{4(G_{swe}-G_{s0})A_{we}z}{z_e^2} & 0 < z < \frac{Z_e}{2} \\ \frac{4(G_{swe}-G_{s0})A_{we}(Z_e-z)}{z_e^2} & \frac{Z_e}{2} < z < Z_e \\ \frac{2(G_{swe-G_{s0}})A_w(z-Z_e)}{(Z_1-Z_e)^2} & Z_e \le z \le Z_1 \\ \frac{2(G_{sB}-G_{s0})A_w(Z_2-z)}{(Z_2-Z_1)^2} & Z_1 \le z \le Z_2 \\ \frac{4(G_{sB}-G_{s0})A_w(z-Z_2)}{(Z_3-Z_2)^2} & Z_2 \le z \le \frac{(Z_2+Z_3)}{2} \\ \frac{4(G_{sB}-G_{s0})A_w(Z_3-z)}{(Z_3-Z_2)^2} & \frac{(z_2+z_3)}{2} \le z \le Z_3 \end{cases} \tag{26}$$

Now we need to determine the gas velocity distribution in the wall region. In the wall–entrance region where

$0 < z < Z_e$, the following boundary conditions can be imposed:

$$U_w|_{r=R} = 0, \quad U_w|_{r=R_w} = U_{ac}, \quad \left.\frac{dU_w}{d_r}\right|_{r=R_w} = 0 \tag{27}$$

which defines a second-order polynomial for the radial distribution of gas velocity as

$$U_w = \frac{U_{ac}R(R-2R_w)}{(R-R_w)^2} + \frac{2U_{ac}R_w}{(R-R_w)^2}r - \frac{U_{ac}}{(R-R_w)^2}r^2 \tag{28}$$

The averaged interstitial gas velocity in the wall region can thus be obtained as

$$U_w = \frac{U_{ac}R(R-2R_w)}{(R-R_w)^2} + \frac{4}{3}\frac{U_{ac}R_w}{(R-R_w)^2}(R^2+RR_w+R_w^2) - \frac{U_{ac}}{2(R-R_w)^2}(R^2+R_w^2) \tag{29}$$

In the wall region above the entrance, we ignore any mass transfer of gas between the wall and core–annulus regions.

Intrinsic correlations

As mentioned earlier, the intrinsic correlations for interzone transport (e.g., F_f's), multiphase interactions (e.g., F_D's) and transport coefficients within the same phase (e.g., C_p's), must be specified in order to solve the coupled set of governing equations. For simplicity, in the consideration of interzone momentum transfer, we only consider the cross-boundary momentum transfer that results from the radial migration of solids whereas the other interfacial momentum transports (such as F_f's) are ignored. Such simplification may be partially justified by the fact that the actual radial distributions of solids phase momentum are continuous.

The momentum transfer between the gas and solids phases in each zone is modeled based on the Richard–Zaki equation,[18] so that

$$F_{Di} = \frac{18\mu}{d_{si}^2} \times \frac{\alpha_{si}}{(1-\alpha_{si})^L} \times (U_i - U_{si}) \tag{30}$$

To account for the effect of the interphase frictional and interparticle collision, an additional term must be included in the momentum equation of solids for solids flows in the dense and acceleration region, which is estimated by[17]

$$\frac{d}{dz}\left(C_{ppi}\frac{dU_{si}}{dz}\right) = \frac{A_i}{U_{si}}\left(\Gamma_i = (U_i - U_{si})\left(-\frac{dP}{dz}\right)\right) \tag{31}$$

The energy dissipation function Γ_i can be further expressed in terms of the solids flow characteristics at minimum transport[17]:

$$\Gamma_i \approx \sum_{j=0}^{N} k_j \alpha_{si}^j \tag{32}$$

Simplified three-zone model

After the implementation of the wall flow model (Flow Characteristics in the Wall Region section) and the intrinsic correlations (Intrinsic Correlations section) into the Three-Zone Model (Three-Zone Modeling section), we can obtain a simplified three-zone model that is summarized as follows:

Mass Balance of Solids

Core-region:

$$\frac{d}{dz}(\alpha_{sc}U_{sc}) = \frac{\dot{m}_{sac}}{\rho_s A_c} \tag{33}$$

Annulus region:

$$\frac{d}{dz}(\alpha_{sa}U_{sa}) = \frac{\dot{m}_{swa} - \dot{m}_{sc}}{\rho_s A_a} \tag{34}$$

Mass Balance of Gas

$$GA - \rho\alpha_w U_w A_w = \rho\alpha_c U_c A_c + \rho\alpha_a U_a A_a \tag{35}$$

Momentum Balance of Gas

Core region:

$$\frac{d}{dz}(a_c U_c^2) = \frac{1}{\rho}\left[-\frac{dp}{dz} - F_{DC} - \alpha_c\rho g\right] \tag{36}$$

Annulus region:

$$\frac{d}{dz}(\alpha_a U_a^2) = \frac{1}{\rho}\left[-\frac{dp}{dz} - F_{DA} - \alpha_a\rho g\right] \tag{37}$$

Momentum Balance of Solids

Core region:

$$\frac{d}{dz}(\alpha_{sc}U_{sc}^2) = \frac{1}{\rho_s}\left[\lambda_c F_{DC} - \alpha_{sc}\rho_s g + \frac{\dot{m}_{sc}U_{sc}}{A_c}\right] \tag{38}$$

Annulus region:

$$\frac{d}{dz}(\alpha_{sa}U_{sa}^2) = \frac{1}{\rho_s}\left[\lambda_c F_{DA} - \alpha_{sa}\rho_s g + \frac{\dot{m}_{sw}U_{sw} - \dot{m}_{sc}U_{sa}}{A_c}\right] \tag{39}$$

Hence we have seven independent equations [(33)–(39)] for seven independent variables (U_{sc}, U_{sa}, α_{sc}, α_{sa}, U_c, U_a, P) in the annulus and core regions.

Experimental Approach

The experimental study provides the experimental data base for validating the proposed three-zone model. Specifically, measurements are made for distributions of solids concentration in all three zones along the tested riser as well as the associated pressure drop distribution along the riser. The solids concentrations are determined from the ECT measurements (with a double-check by optical probe measurements), whereas the pressure drops are measured by a set of differential pressure transducers along the riser.

The riser is an integrated part of a circulating fluidized bed system used in our previous studies,[10] as shown in Figure 6, with an I.D. of 0.1 m and a height of 6.32 m. The solids circulation rate is measured by timing the falling distance of tracer particles in the standpipe. The superficial air velocity is measured by a flow meter. The fluidized particles are FCC catalysts.

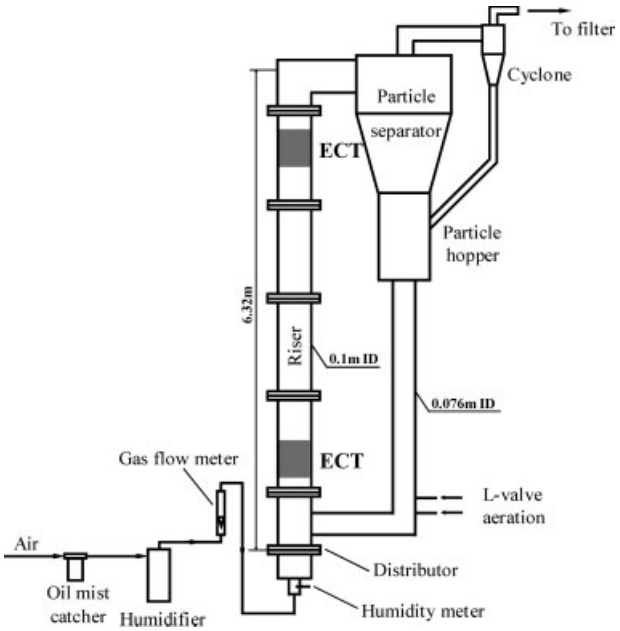

Figure 6. Schematic diagram of the riser system (CFB).

Results and Discussions

Model predictions vs. measurements

To validate our model, the model predictions of solids concentration distributions and pressure distributions are directly compared against the ECT measurements and the pressure drop measurements under the same flow conditions. In this part, two cases of different solids loadings at the same gas velocity are investigated. Specifically, the solids circulation rate is controlled at 1.32 kg/(m^2 s) or 2.30 kg/(m^2 s), whereas the inlet gas velocity is maintained at 0.97 m/s. The averaged solids concentrations in the three zones were measured at five different heights along the riser.

As shown in Figures 7a, b, both measurements and model predictions suggest that the core–annulus–wall structure is built up at the bottom part of the riser and kept stable along the riser. The solid concentrations in each zone at the same height of riser are not only significantly different but also quite different in their distributions along the riser, indicating a fundamental change in hydrodynamic characteristics of solids in different zones. The solid concentrations in the core and annulus regions decrease much faster than that in the wall region in the lower part of the riser. It is interesting to notice that, in the wall region, our model suggests that there exists a peak in solids concentration before it decreases quickly, possibly because of the collision effect between the downwards moving solids from back flow and upwards moving solids from the entrance. Comparison of solids concentration distributions between measurements and model predictions shows the model is quite successful, not only giving excellent qualitative solids distributions of all regions but also yielding very reasonable quantitative results in most of these regions. Figure 8 illustrates the comparison of axial distributions of pressure between the measurements and model predictions, which also shows a very good quantitative agreement.

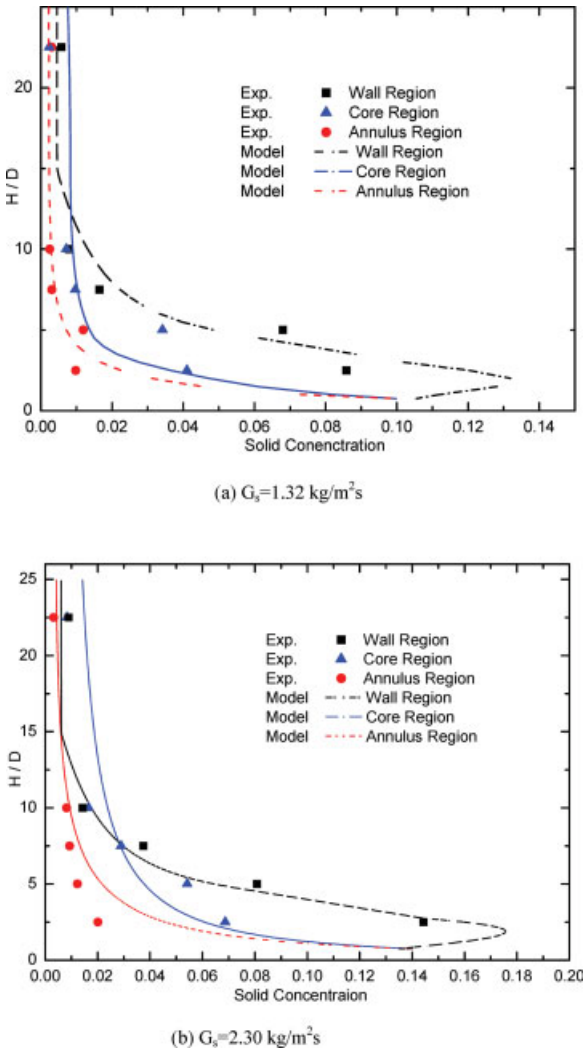

Figure 7. Comparisons of solid concentration distributions (U = 0.97 m/s).

[Color figure can be viewed in the online issue, which is available at www.interscience.wiley.com.]

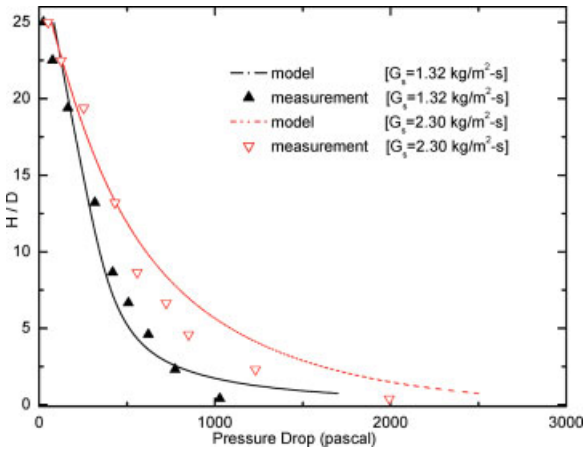

Figure 8. Comparisons of axial distributions of pressure.

[Color figure can be viewed in the online issue, which is available at www.interscience.wiley.com.]

Effect of solids mass flow rate on flow structure

As mentioned earlier, in the riser flow with a low solids mass flow rate, the inwardly migrating solids are all entrained into the flow without any residual solids reaching to the center of the riser. In this case, the riser flow has the familiar "core–annulus" two-zone structure. However, if the solids mass flow rate is increased to such an extent so that some inwardly migrating solids can reach to the center of the riser, the riser flow becomes the "core–annulus–wall" three-zone structure. In order to illustrate the effect of solid circulation rate on flow structure, various riser flows at the same gas velocity but with different solid mass flow rates have been predicted.

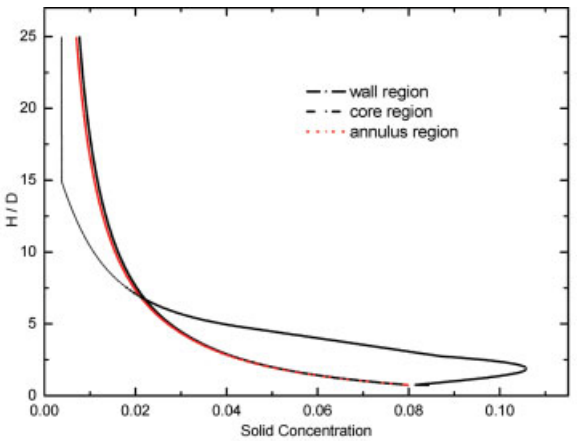

(a) two-zone structure [G_s=4 kg/m^2-s]

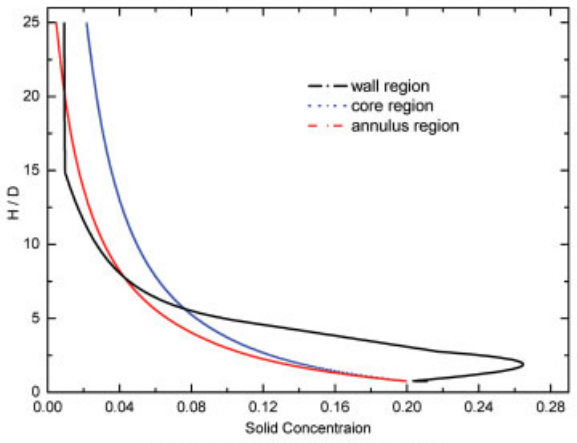

(b) three-zone structure [G_s=10 kg/m^2-s]

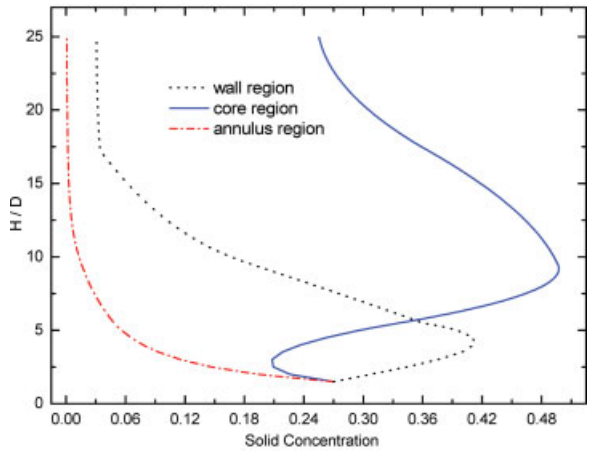

(c) Solid concentration reversal in the core region [G_s=50 kg/m^2-s]

Figure 9. Effect of solid mass flow rate on flow structure.

(a) Two-zone structure [G_s = 4 kg/(m^2 s)]. (b) Three-zone structure [G_s = 10 kg/(m^2 s)]. (c) Solid concentration reversal in the core region [G_s = 50 kg/(m^2 s)]. [Color figure can be viewed in the online issue, which is available at www.interscience.wiley.com.]

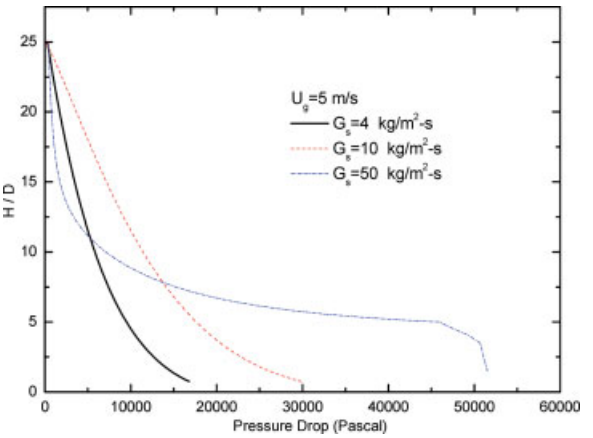

Figure 10. Effect of solids mass flow rate on axial distributions of pressure.

[Color figure can be viewed in the online issue, which is available at www.interscience.wiley.com.]

Figure 9 shows the flow structures of riser flows at a gas velocity of 5 m/s and the solids mass flow rate varying from 4 to 50 kg/(m^2 s). As shown in Figure 9a with a low solids mass flow rate [4 kg/(m^2 s)], the riser flow clearly shows a "core–annulus" two-zone structure, with little difference in solids concentration distributions between the core and annulus regions. With a moderate solids mass flow rate [e.g., 10 kg/(m^2 s)], however, the riser flow becomes a "core–annulus–wall" three-zone structure, with distinct differences in solids concentration distributions among the core, annulus and wall regions, as shown in Figure 9b. The "wall–core–annulus" three-zone structure starts from the entrance of the riser and exits throughout the entire riser. In the dilute transport regime, however, the difference in solids concentration distributions between the core and annulus regions becomes much insignificant, compared to that in the dense transport regime at the bottom of the riser. With a significant increase in solids mass flow rate [e.g., 50 kg/(m^2 s)], as shown in Figure 9c, a reversal-hump-shaped distribution of solids concentration occurs in the core region. The initial decrease of solids concentration is due to the entrance effect on wall boundary layer development, whereas the hump results from a combined effect of a strong immigration of solids to the core region and a much reduced acceleration of the solids in the core region. The formation of the peak solids concentration in the core region can trigger the instability of the "core–annulus–wall" three-zone structure. When the peak solids concentration is high enough, the flow-induced particle–particle interactions (such as wake-induced collisions) will lead to the collapse of the stable structure of solids in the core region, like choking.

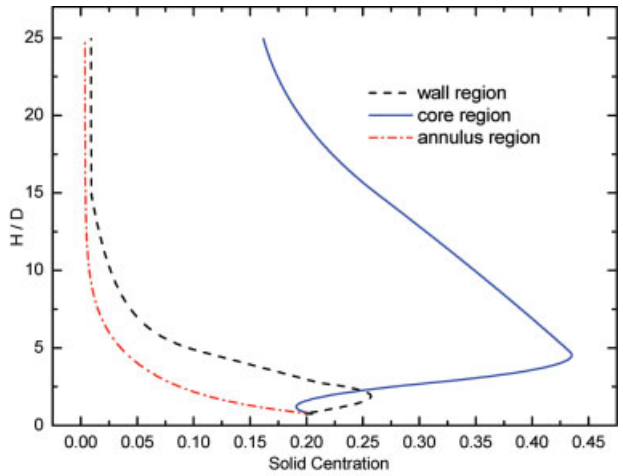

(a) Solid concentration reversal in the core [U=1 m/s]

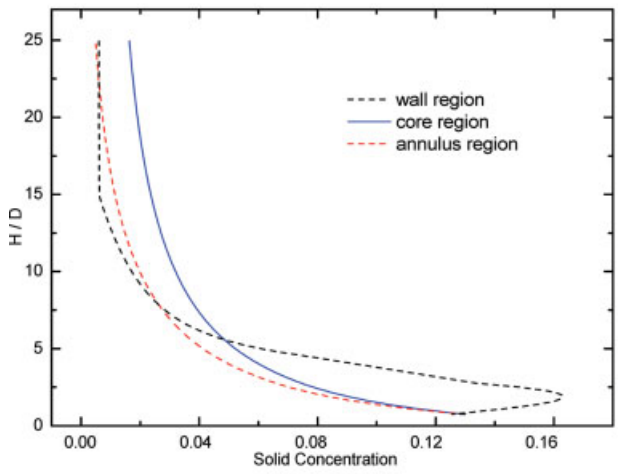

(b) three-zone structure [U=6 m/s]

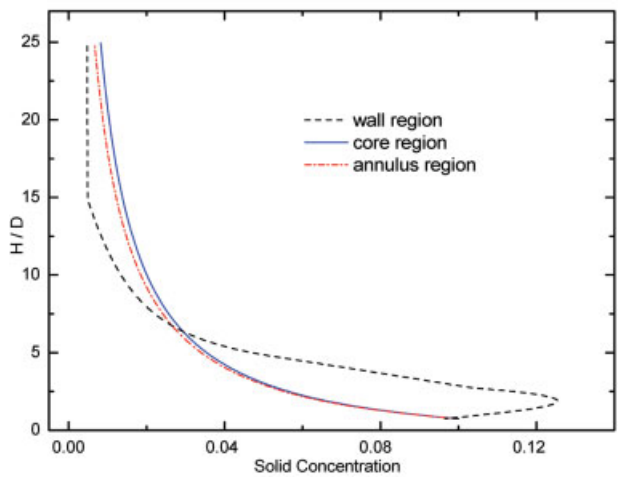

(c) two-zone structure [U = 10 m/s]

Figure 11. Effect of gas inlet velocity on solids concentration structures.

(a) Solid concentration reversal in the core [$U = 1$ m/s]. (b) Three-zone structure [$U = 6$ m/s]. (c) Two-zone structure [U = 10 m/s]. [Color figure can be viewed in the online issue, which is available at www.interscience.wiley.com.]

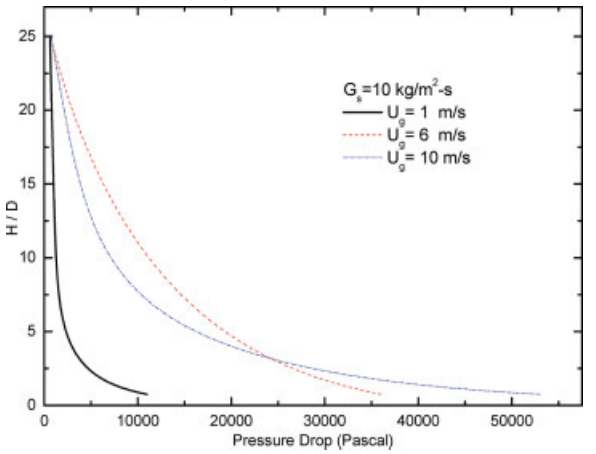

Figure 12. Effect of gas velocity on axial distributions of pressure.

[Color figure can be viewed in the online issue, which is available at www.interscience.wiley.com.]

Figure 10 shows the effect of solids mass flow rate on the axial distributions of pressure. It is interesting to note that, at high solids loadings, even with the solids concentration reversal in the core, there is no reversal in the pressure distribution in a riser flow. This is due to the fact that, in a riser flow, the solids motion is governed by the hydrodynamic driving force (drag force or pressure) rather than inertia.

Effect of inlet gas velocity on flow structure

Besides the solid circulation rate, the gas velocity is another important controlling parameter on the riser flow structure. For riser flows with a given solids mass flow rate, high gas velocities can yield the "core–annulus" two-zone structure, whereas low gas velocities tend to cause the "wall–core–annulus" three-zone structure, even the choking.

Figure 11 shows the riser flow structures at the solids mass flow rate of 10 kg/(m^2 s) and the gas velocity varying from 1 to 10 m/s. As shown in Figure 11a with a low gas velocity (e.g., 1 m/s), the riser flow shows a reversal-hump-shaped distribution of solids concentration occurring in the core region, which is similar to Figure 9c. In this case, the gas velocity is too low to deliver the necessary dilution (or acceleration) of solids against the inwardly migrating solids from the wall. Figure 11b shows that, with an increased gas velocity (e.g., 5 m/s), the riser flow becomes stable with a "wall–core–annulus" three-zone structure. Further increase in gas velocity (e.g., 10 m/s) yields a sufficient hydrodynamic power, not only to make a proper dilution or acceleration of solids but also a sufficient entrainment and dilution of solids emigrated from the wall region. Such hydrodynamic power of gas leads to little difference in solids concentration distributions between the core and annulus regions. Figure 12 shows the effect of gas velocity on axial distributions of pressure.

Conclusions

This article presents a complete mechanistic model to understand the general heterogeneous flow structure in gas–

solid riser flow, especially the "core–annulus–wall" three-zone flow structure and the unstable flow structure that leads to choking. The model prediction results are directly compared with experimental measurement using ECT technology, which shows a fairly good agreement. The proposed mechanisms and corresponding mathematical modeling yield a reasonable explanation for the formation and flow conditions of various heterogeneous structures. Effects of critical flow parameters such as solids mass flow rate and gas inlet velocity have also been illustrated. Simulation results show that the well-known "core–annulus" two-zone structure is easily formed at high gas velocity and/or low solids mass flow rate, and the "core–annulus–wall" three-zone structure always happens at low gas inlet velocity and/or high solids mass flow rate. The formation of reversal solids concentration profiles along the riser in the core region may be the underlying cause of choking.

Notation

List of symbols

A = area
C_{ppi} = transport coefficient
ds = average size of solid particles
F_{Di} = drag force
F_{fii} = friction force
G = flow flux
$\dot{m}_s$ = solids transfer across interface
N = solid number in unit volume
p = pressure
R = riser radius
R_w = wall region radius
U = velocity
z = bed height
α = solid concentration
μ = viscosity
ρ = density
Γ = energy dissipation function
χ = back-mixing ratio (G_{back}/G_s)

Subscripts

a = annulus region
c = core region
g = gas phase
s = solid phase
w = wall region

Acknowledgments

The donors of The Petroleum Research Fund, administrated by the American Chemical Society, are acknowledged for the partial support of this research under the grant of ACS-PRF no. 42759-AC9.

Literature Cited

1. Grace JR, Avidan AA, Knowlton TM. *Circulating Fluidized Beds*, London, UK: Chapman & Hall, 1997.
2. Nakajima M, Harada M, Asai M, Yamazaki R, Jimbo G. Bubble fraction and voidage in an emulsion phase in the transition to a turbulent fluidized bed. In: *Circulating Fluidized Bed III*, Ed., 1991.
3. Brereton CMH, Grace JR. Microstructure aspects of the behavior of circulating fluidized beds. *Chem Eng Sci.* 1993;48:2565–2572.
4. Yates JG, Simons SJR. Experimental methods in fluidization research. *Int J Multiph Flow.* 1994;20:297–330.
5. Rowe PN. Experimental properties of bubbles. In: Davidson JF, Harrison D, editors. *Fluidization* New York: Academic Press, 1971: 121.
6. Schlichthaerle P, Werther J. Axial pressure profiles and solids concentration distribustions in the CFB bottom zone. *Chem Eng Sci*. 1999;54:5485–5493.
7. Horio M, Kuroki H. Three-dimensional visualization of dilutely dispersed solids in bubbling and circulating fluidized beds. *Chem Eng Sci*. 1994;49:2413–2421.
8. Halow JS, Fasching GE, Nicoletti P, Spenik JL. Observations of a fluidized bed using capacitance imaging. *Chem Eng Sci*. 1993; 48: 643–659.
9. Warsito W, Fan LS. Measurement of real-time flow structures in gas-liquid and gas-liquid-solid flow systems using electrical capacitance tomography (ECT). *Chem Eng Sci.* 2001;56:6455–6462.
10. Du B, Warsito W, Fan LS. ECT studies of the choking phenomenon in a gas-solid circulating fluidized bed. *AIChE J*. 2004;50:1386–1406.
11. Bolton LW, Davidson JF. Recirculation of particles in fast fluidized risers. In: Bolton LW, Davidson JF, editors, *Circulation Fluidized Bed Technology II*, Ed. Basu and Large. Toronto: Pergamon Press, 1988.
12. Rhodes MJ, Geldart D. A model for the circulating fluidized bed. *Powder Tech.* 1987;53:155–162.
13. Horio M, Morishita K, Tachibana O, Murata N.Solid distribution and movement in circulating fluidized beds. *In Circulating Fluidized Bed Technology II*, Ed. Basu and Large. Toronto: Pergamon Press, 1988.
14. Senior RC, Brereton CMM. Modeling of circulating fluidized bed solids flow and distribution. *Chem Eng Sci*. 1992;47:281–296.
15. Rhodes MJ, Sollaart M, Wang XS. Flow structure in a fast fluid bed. *Powder Tech.* 1998;99:194–200(7).
16. Zhu C, Yu Q, Fan LS. Modeling on core-annulus-wall structure in circulating fluidized bed riser. *Circulat Fluid Bed Technol*. 2005; VIII:354–360.
17. Zhu C, You J. An energy-based model of gas-solids transport in a riser. *Powder Tech.* 2007;175:33–42.
18. Richardson JF, Zaki WN. Sedimentation and fluidization. *Trans Inst Chem Eng*. 1954;32:35–53.

Manuscript received Mar. 31, 2007, revision received Sept. 26, 2007, and final revision received Feb. 19, 2008.